Sengupta, A. (2019) Electronic and optical properties of $SnX_2$(X=S, Se) - InSe van der Waal's heterostructures from first-principle calculations. *Physica Scripta*, 94(12), 125806. (doi: 10.1088/1402-4896/ab3bb3)

There may be differences between this version and the published version. You are advised to consult the publisher's version if you wish to cite from it.

http://eprints.gla.ac.uk/194221/

Deposited on 29 August 2019

Enlighten – Research publications by members of the University of Glasgow
http://eprints.gla.ac.uk

# Electronic and optical properties of $SnX_2$ (X=S, Se) - InSe van der Waal's heterostructures from first-principle calculations

Amretashis Sengupta1*†

[1]Indian Institute of Engineering Science and Technology, Shibpur, Howrah – 711 103, India

***Corresponding author, E-mail:** amretashis@gmail.com

***Abstract:***

***Abstract:*** *In this work from first-principles simulations we investigate bilayer van der Waal's heterostructures (vdWh) of emerging 2-dimensional (2D) optical materials $SnS_2$ and $SnSe_2$ with monolayer InSe. With density functional theory (DFT) calculations, we study the structural, electronic, optical and carrier transport properties of the $SnX_2$ (X=S,Se)-InSe vdWh. Calculations show $SnX_2$-InSe in its most stable stacking form (named AB-1) to be a material with a small (0.6-0.7eV) indirect band-gap. The bilayer vdWh shows broad spectrum optical response, with number of peaks in the infra-red to visible region. In terms of carrier transport properties, asymmetry in conductance was observed with respect to the transport direction and electron and hole transmission. The findings are promising from the viewpoint of nanoelectronics and photonics.*

**Keywords: 2D materials, heterostructures, DFT, RPA**

## I. Introduction

Layered tin dichalcogenides such as $SnS_2$ and $SnSe_2$ have recently been in focus for their novel properties [1]-[6] such as indirect to direct band-gap transition [1,5], strain tunable magnetism [3] , high carrier mobility [2], low thermal conductivity [2], fast photoresponse [1] etc. These properties indicate wide-ranging potential applications of 2-dimensional (2D) $SnX_2$ (X=S,Se) in sensors, nanoscale FETs, thermoelectrics, catalysis, solar cells and photonic devices. [4,5,6] The industrial viability of these materials are enhanced by the choice of large number of chemical and physical synthesis techniques for layered $SnX_2$ [1]-[6] and the relative abundance and environmental friendliness of the constituent elements [1].

Also, another emerging material, layered InSe has shown good band-gap tunability and carrier transport properties [7]-[12] and good photo-detection and novel optical response wherein the band edge response is absent in monolayers [7,8]. As a result layered or 2D InSe is also being pursued for nanoelectronics and photonics in a significant manner. [11,12]

---

†The author was with the Indian Institute of Engineering Science and Technology, Shibpur at the time of carrying out this work. Presently he is with the School of Engineering, University of Glasgow, Glasgow G12 8QQ, United Kingdom.

Monolayer InSe has an experimentally reported lattice parameter of about 4.09Å [11], while single layer 2H-$SnS_2$ and 2H-$SnSe_2$ have lattice parameters around 3.63Å and 3.81Å respectively. [13] This indicates a much smaller lattice mismatch for $SnX_2$-InSe than that of InSe with TMDs such as $MoS_2$ (a=3.15Å), $MoSe_2$ (a=3.32Å), $WS_2$ (a=3.19Å) and $WSe_2$ (a=3.33Å). [14]-[16]

With the recent growing interest in vdWh structures, bilayer heterostructures of InSe-$MX_2$ (M=Mo, W, X= S, Se) have been reported both experimentally and theoretically. [15,16,17] A number of other 2D materials as SnS (a=4.28Å, b=4.08Å), GeS (a=4.28Å, b=3.97Å) and phosphorene (a=3.30Å, b=4.62Å) have also been theoretically explored as vdWh materials in combination with InSe. [18, 19]

However, to the best of the author's knowledge the present work is the first report to study in detail the vdWh of $SnX_2$-InSe. In terms of fabrication process a better lattice matching can offer possibilities of growing one material on top of another in addition to transfer based techniques. Further, standalone $SnX_2$ have shown novel properties as high carrier mobility [2], low thermal conductivity [2], fast photoresponse [1] etc which may work in synergy with a material such as InSe.

Thus, possessing excellent lattice matching, 2D hexagonal $SnX_2$ and InSe have very good potential compatibility in sequentially grown superlattices or van der Waals heterostructures (vdWh). Such a combination, could offer interesting optical and electronic properties, owing to the close values of band-gaps resulting in a high possibility of intra and inter-band transitions among the two different materials.

In this work we look to investigate $SnX_2$-InSe vdWh from first principle density functional theory (DFT) simulations. We identify the most stable stacking of the vdWh lattice and thereafter calculate the electronic properties and various optical properties as joint density of state (JDOS), complex dielectric functions and energy loss spectra (theoretical electron energy loss spectra or EELS), of the same. Also we investigate the carrier transport properties in such vdWh by means of non-equilibrium Green's function (NEGF) simulations.

## II. Methodology

We employ generalized gradient approximation (GGA) calculations with Perdew-Burke-Ernzerhoff (PBE) exchange and correlation functional [20] in the Quantum ESPRESSO package [21]. The vdWh unit cells consisting of $SnX_2$-InSe had 15Å vacuum gap, and they were sampled with a 9x9x1 Monkhorst-Pack [22] k-point grid, with a cutoff energy of 150Ry. The Davidson diagonalization algorithm [23] was used in the calculations, with convergence threshold of $10^{-7}$ Ry. The fhi88pp norm-conserving basis sets of Troullier-Martins type [24,25] were used in the calculations. The van der Waals corrections were included by the Grimme's DFT-D2 method [26] and the structures were

relaxed with Broyden-Fletcher-Goldfarb-Shanno (BFGS) algorithm [27] for variable cell relaxation to a pressure convergence threshold of 0.5kBar and with Hellmann-Feynman forces reduced to less than $10^{-4}$Ry/Bohr.

The optical spectra of the systems were calculated with the random phase approximation (RPA) approach, as implemented in the epsilon.x toolset [28] The joint density of states (JDOS) is defined as [28]

$$J(\omega)=\sum_{\alpha}\sum_{\beta}\frac{V}{(2\pi)^3}\int\delta\left(E_{k,\beta}-E_{k,\alpha}-\hbar\omega\right)\left[f(E_{k,\alpha})-f(E_{k,\beta})\right]\cdot d^3k \tag{1}$$

$V$ is the volume of the cell, $\alpha,\beta$ are states belonging to conduction and valence bands respectively, $E_{k,}$ are the eigenvalues of the Hamiltonian and $f(.)$ is the Fermi distribution function. The Dirac delta function is approximated by a Gaussian distribution, normalized to one [28]

$$G(\omega)=\frac{1}{\Gamma\sqrt{\pi}}\exp\left\{\left(E_{k,\beta}-E_{k,\alpha}-\hbar\omega^2\right)/\Gamma^2\right\} \tag{2}$$

$\Gamma$ is the broadening parameter. The complex dielectric function is given by [28]

$$\begin{aligned}\varepsilon_2(\omega)=1-\frac{4\pi q^2}{VN_k m^2}\sum_{\alpha,k}\frac{df(E_{k,\alpha})}{dE_{k,\alpha}}\frac{\hat{M}_{\mathrm{a,b}}}{\omega^2+i\eta_1\omega}+\ldots\\ \ldots+\frac{8\pi q^2}{VN_k m^2}\sum_{\alpha\neq\beta}\sum_{k}\frac{\hat{M}_{\mathrm{a,b}}}{(E_{k,\beta}-E_{k,\alpha})}\frac{f(E_{k,\alpha})}{(\omega_{k,\beta}-\omega_{k,\alpha})^2+\omega^2+i\eta_2\omega}\end{aligned} \tag{3}$$

$\eta_1$ and $\eta_2$ are the inter-band and intra-band smearing respectively. The matrix element $M_{a,b}$ are defined as [28]

$$\hat{M}_{a,b}=\left\langle u_\beta\mid p_a\mid u_\alpha\right\rangle\left\langle u_\alpha\mid p_b{}^{\dagger}\mid u_\beta\right\rangle \tag{4}$$

With a London transformation upon $\varepsilon_2$ the dielectric tensor calculated on the imaginary frequency axis may be written as [28]

$$\varepsilon_2(i\omega)=1+\frac{2}{\pi}\int_0^{\infty}\frac{\omega'\varepsilon_2(\omega')}{\omega'^2+\omega^2}d\omega' \tag{5}$$

The energy loss spectrum (theoretical EELS count) is obtained from the imaginary part of the inverse dielectric tensor.

The transmission is calculated with the DFT-NEGF method [29]-[35] in QuantumWise ATK 2016.4 [26], using similar DFT simulation parameters as with the Quantum ESPRESSO calculations. For the NEGF transport calculation, an FFT2D Poisson solver and Krylov self-energy calculator are

employed in ATK. [33]-[35] The detailed DFT-NEGF transport calculation methodology is well-described in literature [29]-[35] The zero-bias transmission spectra were evaluated for both the zigzag and the armchair direction. The Green's function can be expressed as [29]-[35]

$$G(\mathrm{E}) = \left[ (\mathrm{E} + i\delta)S - H - \Sigma^{R}(\mathrm{E}) - \Sigma^{L}(\mathrm{E}) \right]^{-1} \tag{6}$$

In (X) $H$ is the Hamiltonian, and $S$ is the overlap matrix. $\delta$ is an infinitesimally small positive quantity. The self-energy matrices of the right/left contacts is $\Sigma^{\mathrm{R,L}}$ and is related to the broadening matrix $\Gamma$ as [29]-[31]

$$\Gamma = i\left(\Sigma - \Sigma^{\dagger}\right) \tag{7}$$

The transmission can be calculated from the Green's function as [29,30,35]

$$T(\mathcal{E}) = \mathrm{Tr}\left[ G\Gamma^{R}G^{\dagger}\Gamma^{L} \right] \tag{8}$$

## III. Results and Discussions

The hexagonal monolayer $SnX_2$ has the Sn atom sitting at the centre of edge sharing octahedral and lying between two layers of chalcogen atoms. Such a structure when combined with the corrugated surface of the InSe monolayer, presents various possible configurations. Considering the three high symmetry points in the hexagonal lattice and three dissimilar atoms in the $SnX_2$ layer (in terms of element as well as position), and the corrugated nature of the InSe with two (chemically) distinguishable crystallographic positions, there can be in total 12 different possible structures of the $SnX_2$-InSe vdWh. They are labelled as AA stacking (4 types), AB stacking (2 types) and AC stacking (6 types).

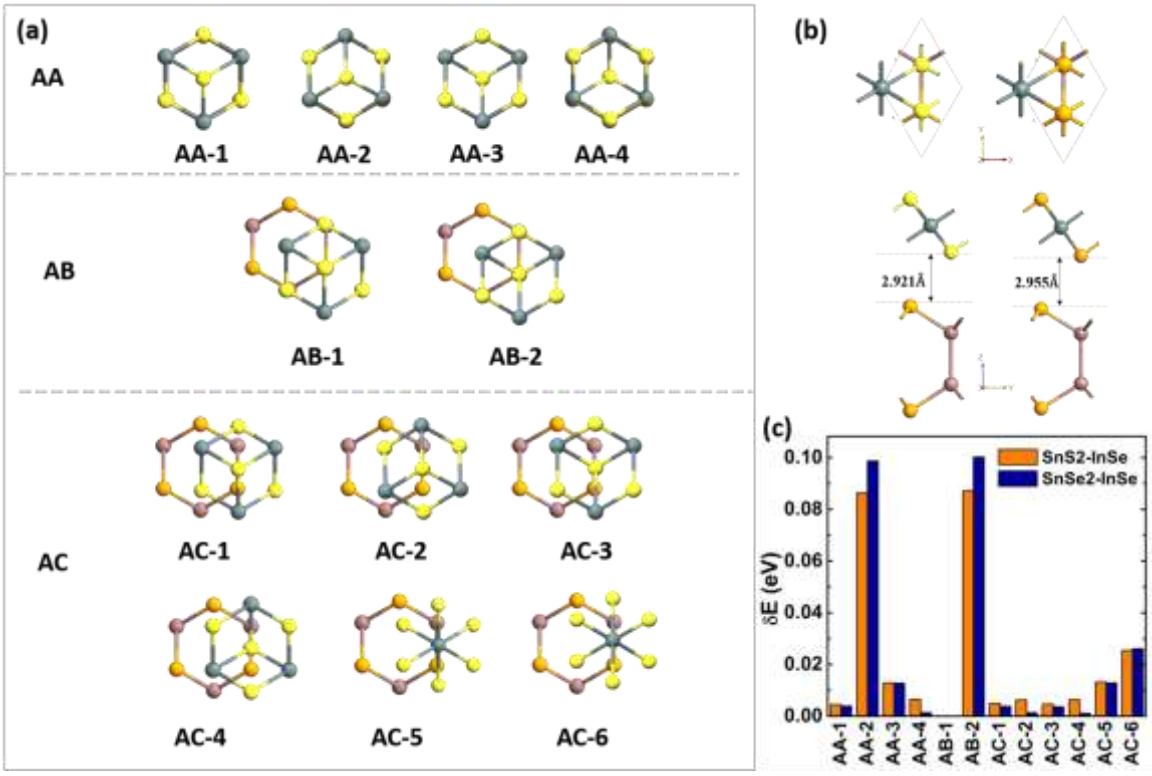


**Fig. 1: (a)** The top views (xy-plane) of the different possible stacking structures structures of the $SnX_2$-InSe vdWh unit-cell **(b)** The top (*xy*-plane) and side (*yz*-plane) view of the most stable structure unit-cell (AB-1) and **(c)** the relative total energies with respect to the most stable structure. Structural details are presented more elaborately in the supplementary material [36]

The optimized cell parameters of the different structures are provided in Table I. Of the different structures the AB-1, is the most stable, for both $SnS_2$-InSe and $SnSe_2$-InSe vdWh structures. In this structure the top chalcogenide atom of $SnX_2$ lies directly over the top Se atom of InSe while the bottom chalcogenide atom of $SnX_2$ lies over the top In atom. While there are other structures as well which differ only by a very small amount of energy in terms of stability, we look to focus mostly on the most energetically stable configuration in the further studies. In the supplementary material [36] elaborate figures with the top view (xy plane) and the side view (yz plane) of the 12 possible structures for $SnX_2$-InSe vdWh are presented. To make the stacking easily understandable, a 4x4 supercell is used for visualization purposes in the supplementary material.

**Table I:** Different structures of the $SnX_2$-InSe vdWh and associated lattice parameters and interlayer spacing.

| Stacking type | Lattice parameter a (Å) | | Interlayer spacing d (Å) | |
|---|---|---|---|---|
| | $SnS_2$-InSe | $SnSe_2$-InSe | $SnS_2$-InSe | $SnSe_2$-InSe |
| AA-1 | 3.8139 | 3.8894 | 2.9777 | 2.9704 |
| AA-2 | 3.8098 | 3.8802 | 3.7131 | 3.7756 |
| AA-3 | 3.8139 | 3.8919 | 2.9777 | 2.9772 |

| | | | | |
|---|---|---|---|---|
| AA-4 | 3.8138 | 3.8868 | 2.9758 | 2.9375 |
| AB-1 | 3.8133 | 3.8912 | 2.9213 | 2.9548 |
| AB-2 | 3.8086 | 3.8801 | 3.7196 | 3.7849 |
| AC-1 | 3.8114 | 3.8846 | 3.0642 | 3.1113 |
| AC-2 | 3.8115 | 3.8856 | 3.037 | 3.0857 |
| AC-3 | 3.8113 | 3.8853 | 3.0681 | 3.1131 |
| AC-4 | 3.8119 | 3.8858 | 2.8639 | 2.9106 |
| AC-5 | 3.8154 | 3.8843 | 3.0677 | 3.1124 |
| AC-6 | 3.8056 | 3.8766 | 3.091 | 3.1488 |

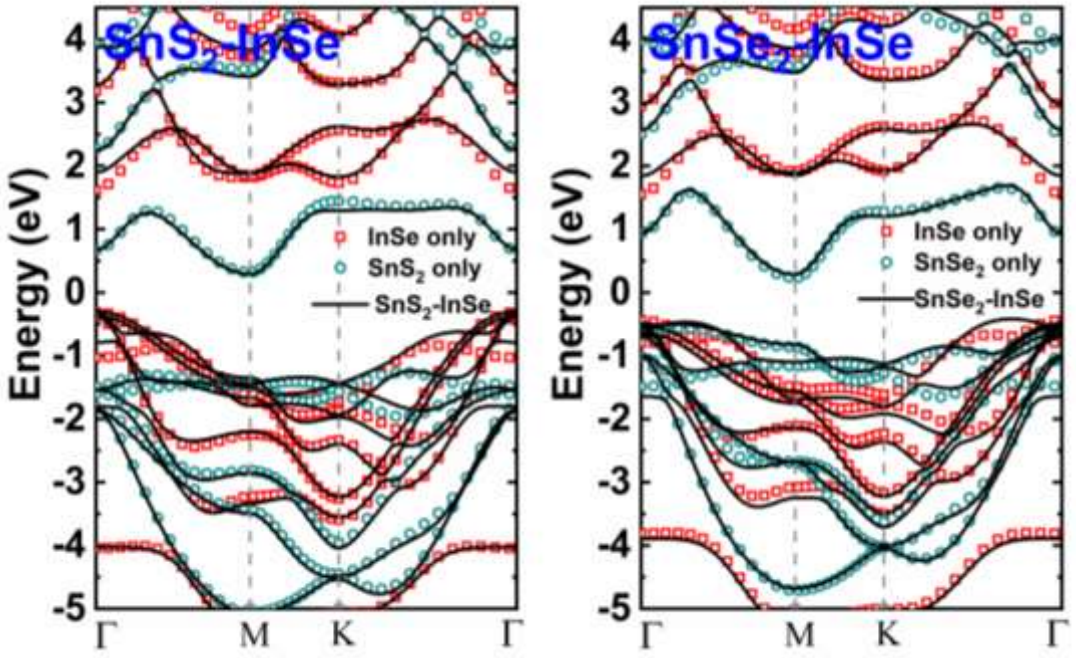


**2. (a)**

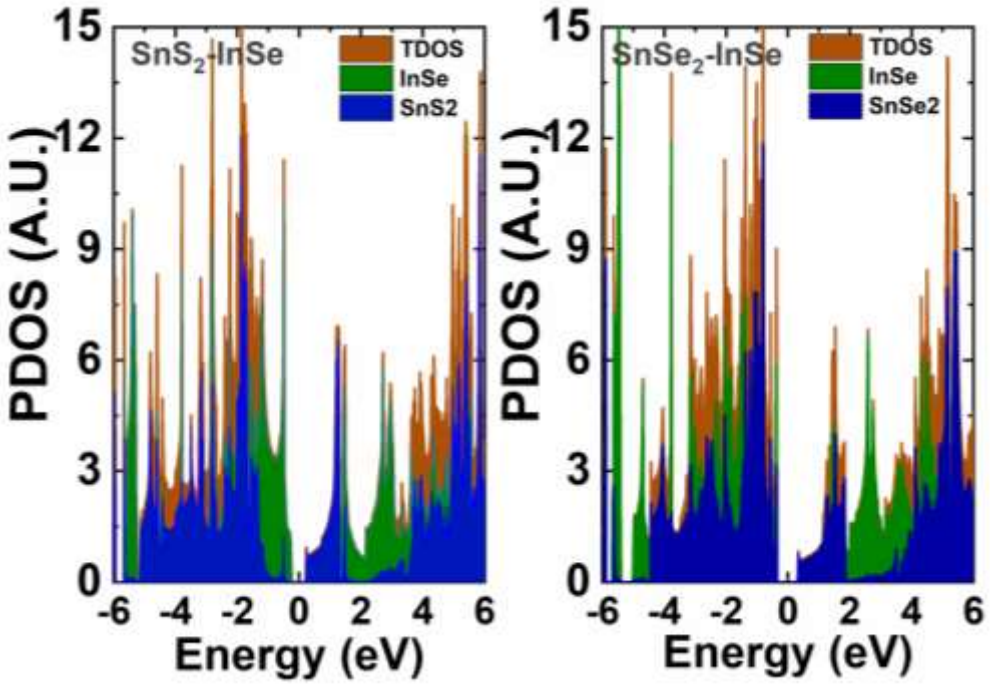


**2. (b)**

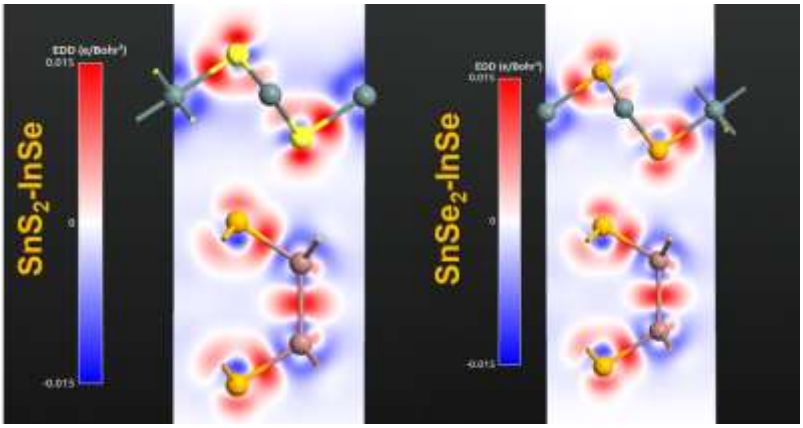


**2. (c)**

**Fig. 2 : (a)** PBE Bandstructures of the $SnX_2$-InSe vdWh, showing also the contribution of the comprising layers in dashed lines. **(b)** Projected Density of states (PDOS) plots showing the contributions of the individual layers and the resulting total DOS in the vdWh. **(c)** Electron density difference (EDD) plots for the vdWh

In Fig. 2a, the bandstructures of the most stable form (AB-1 stacking) of the $SnS_2$-InSe and the $SnSe_2$-InSe vdWh are presented. The plots also show the contribution of individual layers to the overall bandstructure. The contributions are inclusive of the small strain that is incurred due to formation of the vdWh. This is done by calculating the bandstructure for each component at a time by removing the other layer from the optimized cell. Thus, the effect of the interlayer interaction (independent of the strain) can also be very clearly understood.

The calculated bandstructures for the most stable structure is shown in Fig. 2a. Both the vdWh show indirect band-gap. $SnS_2$-InSe shows a gap of 0.61eV between M point in conduction band (CB) and Γ point in valence band (VB). $SnSe_2$-InSe has a slightly larger gap of 0.70, with the CB minima at M point and VB maxima at a point in the K-Γ path, located about two third the distance from K to Γ point. Such gaps offer good possibilities for keeping electron and hole distributions apart.

From the bands, we see that the conduction band (CB) minima in both the vdWh are contributed by the CB from the $SnX_2$ layer, and are located at the M point of the hexagonal Brillouin zone. However the valence band (VB) maxima, is contributed mostly by the InSe. Among the band extrema, for $SnSe_2$, the VB maxima, located between K and Γ, seems to be affected more by the interlayer interactions. It is here that the $SnSe_2$ contribution seems to be influenced more to interlayer interactions, thus giving rise to the VB maxima of the vdWh. In general, around the Γ point the lowest conduction bands of the InSe also seem to be affected by interlayer interactions by vdWh formation.

For the carrier mobility, it can be qualitatively said that as the CB min in the vdWh is contributed by $SnX_2$, it possesses a slightly lesser curvature against that of intrinsic InSe. This indicates a slightly higher effective mass and as a result a slightly lesser electron mobility as compared to pure InSe. The case of the hole mobility is expected to remain more or less the same for $SnS_2$-InSe vdWh considering the band profile of vdWh at VB max (Γ point) which is almost identical to that for the InSe. For $SnSe_2$-InSe however the hole mobility is expected to degrade as the vdWh VB maxima is now much flatter in compared to that of InSe.

The PDOS plots in Fig. 2b show the vdWh conduction bands to be more influenced by the $SnX_2$ layer. However for the valence band (VB) maxima, the $SnX_2$ contribution seems to depend on chalcogen of the top layer (X=S or Se). PDOS reveals that it is InSe that has more contribution to VB edges in $SnS_2$-InSe as compared to $SnS_2$, while for $SnSe_2$-InSe vdWh, it is $SnSe_2$ which contributes more significantly to the VB states. Such different type of contributions push the VB max upwards at Γ point in case of $SnS_2$-InSe and somewhere between the K and Γ points for $SnSe_2$-InSe vdWh.

The difference in the charge distribution or transfer in the two vdWh is investigated with electron density difference (EDD) analysis, presented in Fig 2c. The more positive EDD around the chalcogen atoms of the $SnX_2$ in case of $SnS_2$-InSe, as compared to $SnSe_2$-InSe, indicates a stronger tendency for electron accumulation near the S atoms in $SnS_2$ than the Se atoms in $SnSe_2$ vdWh. Apart from this a tendency of developing a stronger dipole moment between the Sn-S pair as compared to the Sn-Se pair is also evident from the EDD plot. These factors revealed by the PDOS and the EDD results contribute to the bandstructure differences among the two vdWh.

The carrier effective masses ( $m^*$ ) for the vdWh were calculated with a polynomial fitting formula, considering the parabolic band approximation and using the relation $\frac{1}{m^*} = \frac{1}{\hbar^2}\left(\frac{d^2\xi}{dk_i dk_j}\right)$ , $\xi$ being the energy eigenvalue and $k_{i,j}$ the wave-vector along $i, j$ direction at the VB maxima and the CB minima in the (100) and (010) directions. The calculated effective masses are listed in Table-II.

**Table II:** The calculated band gap and carrier effective mass for the vdWh

| vdWh | Band gap $E_g$ (in eV) | electron effective mass ( $m_e^*$ ) | | hole effective mass ( $m_h^*$ ) | |
|---|---|---|---|---|---|
| | | (100) | (010) | (100) | (010) |
| $SnS_2$-InSe | 0.61 (Indirect) | 0.572 $m_0$ | 0.675$m_0$ | 0.897 $m_0$ | 0.795$m_0$ |
| $SnSe_2$-InSe | 0.70 (Indirect) | 0.653 $m_0$ | 0.789$m_0$ | 0.956 $m_0$ | 0.992$m_0$ |

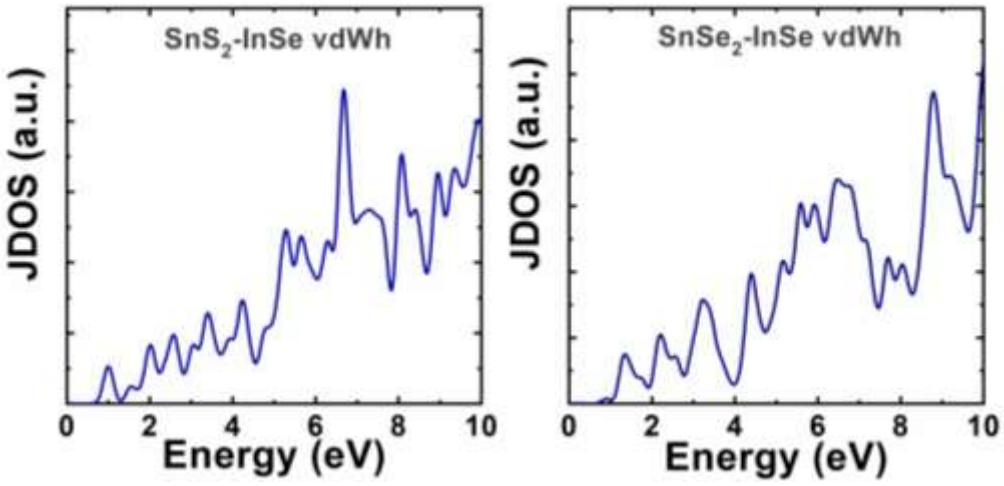


**Fig 3:** The calculated joint density of states (JDOS) of the $SnX_2$-InSe vdWh.

The calculated optical joint density of states (JDOS) of the vdWh are presented in Fig. 3. JDOS gives a qualitative idea of how many allowed optical transitions may exist between the populated valence states and the unpopulated conductions states having energy difference of $\hbar\omega$ . As JDOS is an indicator of the number of available states for photons to interact with, for optical emission/absorption process, it is an important part of optical characteristics of a given material. The JDOS of the two structures differ in the sharpness of the peaks apart from their position and also the number of peaks. While the $SnS_2$-InSe shows a greater number of sharper peaks, the JDOS peaks for $SnSe_2$-InSe are more spread-out in nature, and also lesser in number. A cascade of small but well defined peaks in the range 0.5-5eV for $SnS_2$-InSe vdWh outnumbers those in $SnSe_2$-InSe. Around the 1eV energy range,

$SnS_2$-InSe shows more possible transitions than $SnSe_2$-InSe. Also around a higher energy of 6.5-7.5eV, there exists a significant difference in terms of the JDOS among the two vdWh. The $SnSe_2$-InSe vdWh is characterised by a significant decline in the JDOS around the 7-8eV energy range.

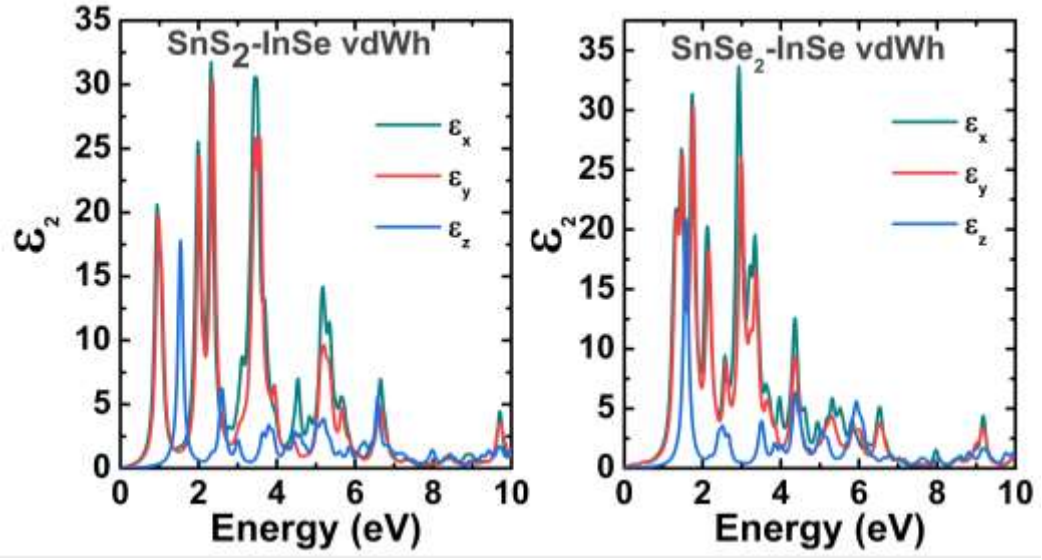


**Fig 4:** The calculated imaginary part of the complex dielectric function of the $SnX_2$-InSe vdWh.

The imaginary part of the complex dielectric function ( $\varepsilon_2$ ), which can also act as a measure of optical absorption, is presented in Fig. 4. The two in-plane components (*x* and *y*) and the out-of plane (z) component are all shown in the plots. In perfectly isotropic bulk materials all the three components should be the same, however for heterostructures or interfaces this is seldom the case. In monolayers or vdWh assuming the light to be incident from the out-of-plane z direction, polarization is created in the in-plane x and y direction by the incident irradiation. [37] As there exist anisotropy among x and y direction of the vdWh (e.g. in terms of the structural and electronic properties as effective mass etc.), $\varepsilon_x$ and $\varepsilon_y$ differ from each other. A stronger absorption in the infrared (IR) to visible range is observed for both the vdWh. For both the structures, the *z*-component of $\varepsilon_2$ appears blue-shifted as compared to the in-plane (*x* and *y* components). The blue-shift is more prominent in case of the $SnS_2$-InSe vdWh. Considering the position of the in-plane characteristics, more discrete peaks at lower energies between 0.75-2.5eV can be observed for $SnS_2$-InSe as compared to $SnSe_2$-InSe vdWh. The peaks in case of the $SnSe_2$-Inse vdWh are more concentrated together, in the lower energy ranges. These corroborate with the JDOS spectra discussed previously. The spike in available states in $SnS_2$-InSe for transition around the 6.5eV mark, is also well reflected by the presence of a stronger response in this region by the $SnS_2$-InSe vdWh, as compared to $SnSe_2$-InSe vdWh.

The strongest peak for both $\varepsilon_x$ and $\varepsilon_y$ in $SnS_2$-InSe vdWh is seen around 2.33eV energy, while for $\varepsilon_z$ it is around 1.54eV. For $SnSe_2$-InSe vdWh however, the strongest peak for $\varepsilon_x$ lies around 2.95eV, while that for $\varepsilon_y$ is situated around 1.75eV and for $\varepsilon_z$ at 1.59eV.

Here it must also be mentioned that the results presented herein are based on a random-phase approximation (RPA) method as described by Benassi et. al. [28]. This implementation based on a multi-particle approach and offers superior accuracy over simulations with the single particle dielectric tensor. However, it does not include the excitonic effects for which GW and Bethe-Salpeter Equation (BSE) calculations could yield better results. That being said, considering the huge computational cost for GW-BSE calculations, the results presented herein can be considered a at least a good pointer towards the optical response of the vdWh systems under consideration.

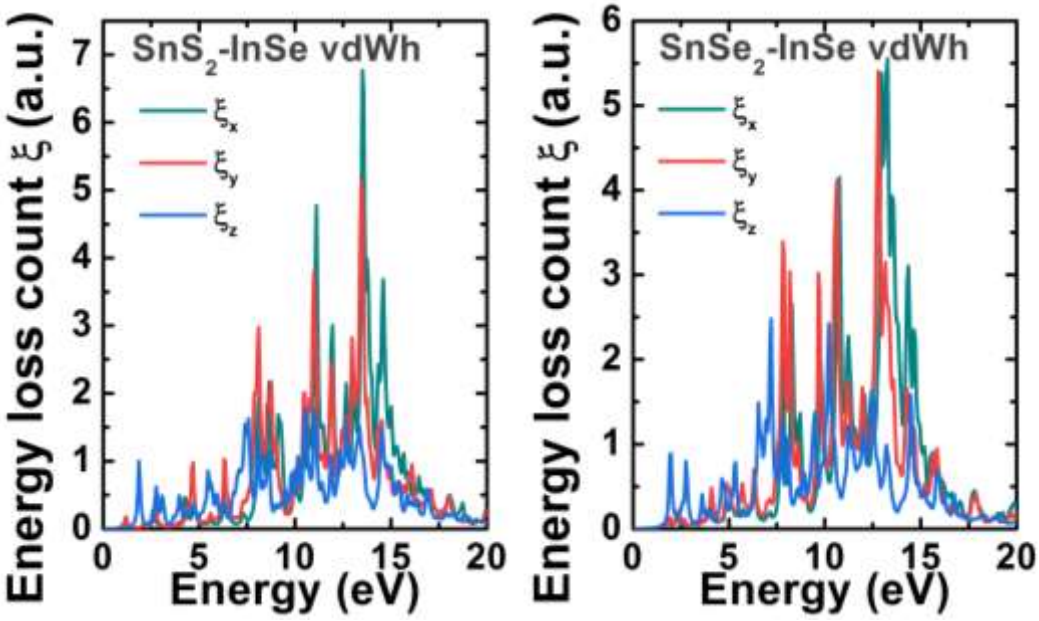


**Fig 5:** The energy loss spectra of the $SnX_2$-InSe vdWh.

The theoretical EELS count is presented in Fig. 5, shows the maxima for the $SnS_2$-InSe vdWh at 13.27, 12.79 and 7.21eV for the *x*, *y* and *z* components respectively. For the $SnSe_2$-InSe vdWh, the same are observed at 13.51, 13.45 and 10.57eV. The bulk plasmon frequency for these systems can thus be estimated to be $8.94 \times 10^4$ $cm^{-1}$ and $1.01 \times 10^5$ $cm^{-1}$ for $SnS_2$-InSe and $SnSe_2$-InSe vdWh respectively.

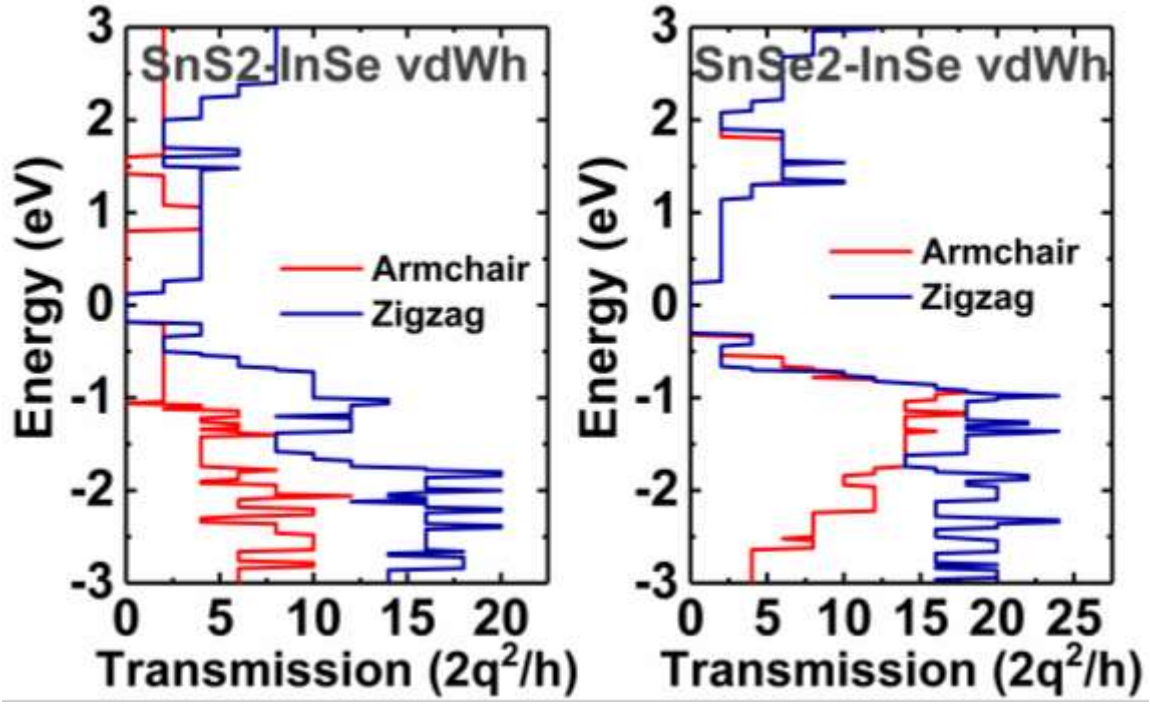


**Fig 6:** The carrier transmission spectra of the $SnX_2$-InSe vdWh.

The transmission spectra of both of the vdWh show an enhanced carrier transport properties for the valence bands rather than the conduction bands. Also observable is the asymmetry in conductance in the armchair and the zigzag direction of the $SnX_2$-InSe structures. The suppression of transport in the armchair direction than that in the zigzag direction is more significant for the $SnS_2$-InSe vdWh, than the $SnSe_2$-InSe vdWh. However the magnitude of transmission for holes in both transport directions is more in case of the $SnSe_2$-InSe structure. For electron transport there exist very little asymmetry on the transport direction for $SnSe_2$-InSe vdWh, as compared to $SnS_2$-InSe, additionally the magnitude for the zigzag direction, is also quite close for both the vdWh. While the asymmetry may be attributed to the disparity in carrier effective masses in the different transport directions, the enhanced hole conduction is a result of the larger number of valence states available near the Fermi-level (as visible in the DOS). The asymmetry in terms of transport direction and electron/ hole transmission, is something that can be utilized for novel applications in photonic and electronic devices based on $SnX_2$-InSe vdWh.

## IV. Conclusion

In this work by density functional theory simulations the structural, electronic and optical properties of bilayer van der Waals heterostructures made of 2D $SnX_2$ (X=S,Se) and InSe were investigated. Among the 12 different possible stacking combinations AB-1 stacking, was found to be the most

stable for both the vdWh. The stable vdWh structures were thereafter studied for their bandstructure, DOS, JDOS and other optical parameters such as the imaginary dielectric function and theoretical EELS spectra. It was observed that $SnS_2$-InSe and $SnSe_2$-InSe vdWh form indirect-gap materials with small PBE band-gap values of 0.61 and 0.70eV respectively. The vdWh also showed moderate electron and hole effective masses ranging between 0.57-0.78$m_0$ and 0.79-0.99$m_0$ respectively depending upon the material and the transport directions. A good optical response could be observed in the IR-visible range for both the $SnX_2$-InSe vdWh, with the peaks in the dielectric function being more closely packed and also slightly blue shifted for the $SnSe_2$-InSe as compared to $SnS_2$-InSe. A drop in JDOS and optical response could be observed around 6-6.5eV and 6.75eV for the $SnSe_2$-InSe, as compared to its $SnS_2$ counterpart. The bulk plasmon frequency was estimated to be around $8.94x10^4$ and $1.0x10^5$ $cm^{-1}$ for $SnS_2$ and $SnSe_2$ based vdWh respectively. Carrier transport computed with the DFT-NEGF method, showed asymmetric conductance in terms of transport direction (armchair / zigzag) and the nature of carriers (electrons/ holes). The optical and transport properties calculated show good prospect of application of $SnX_2$-InSe vdWh studied in this work, in photonics and nanoelectronics. The excellent lattice matching and environmental stability of the constituent 2D materials, make a good case for not only bilayer but for multi-layer $SnX_2$-InSe devices.

**V. Acknowledgements**

The author wishes to thank Department of Science and Technology, Govt. of India for DST INSPIRE Faculty Grant No. IFA-13 ENG- 62.

## References

[1] L.A. Burton, T. Whittles, D. Hesp, W.M. Linhart, J.M. Skelton, B. Hou, R. Webster, G. O'Dowd, R. Christian, D. Cherns, D.J. Fermin, T. Veal, V. Dhanak, A. Walsh, Electronic and optical properties of single crystal SnS2: an earth-abundant disulfide photocatalyst, J. Mater. Chem. A. 4 (2016) 1312–1318.

[2] A. Shafique, A. Samad, Ultra low lattice thermal conductivity and high carrier mobility of monolayer SnS2 and SnSe2: a first principles study, Phys. Chem. Chem. Phys. 19 (2017) 20677–20683.

[3] H. Xiang, B. Xu, Y. Xia, J. Yin, Z. Liu, Strain tunable magnetism in SnX 2 ( X = S , Se ) monolayers by hole doping, 2 (2016) 1–8.

[4] Y. Li, S.G. Leonardi, A. Bonavita, G. Neri, W. Wlodarski, Two-Dimensional (2D) SnS2-based Oxygen Sensor, Procedia Eng. 168 (2016) 1102–1105. doi:10.1016/j.proeng.2016.11.355.

[5] J. Li, J. Shen, Z. Ma, K. Wu, Thickness-controlled electronic structure and thermoelectric performance of ultrathin SnS2 nanosheets, Sci. Rep. (2017) 1–9.

[6] T. Yang, B. Zheng, Z. Wang, T. Xu, C. Pan, J. Zou, X. Zhang, Z. Qi, H. Liu, Y. Feng, W. Hu, F. Miao, L. Sun, X. Duan, A. Pan, Van der Waals epitaxial growth and optoelectronics of large-scale WSe2/SnS2 vertical bilayer p–n junctions, Nat. Commun. 8 (n.d.) 1906.

[7] D. A. Bandurin *et al.*, High electron mobility , quantum Hall effect and anomalous optical response in atomically thin InSe, *Nat. Nanotechnol.*, pp. 1–6, 2016.
[8] G. W. Mudd et al., High Broad-Band Photoresponsivity of Mechanically Formed InSe – Graphene van der Waals Heterostructures, Adv. Mater., vol. 27, pp. 3760–3766, 2015.
[9] S. Lei et al., Evolution of the electronic band structure and efficient photo-detection in atomic layers of InSe, ACS Nano, vol. 8, no. 2, pp. 1263–1272, 2014.
[10] G. W. Mudd et al., Tuning the bandgap of exfoliated InSe nanosheets by quantum confinement, Adv. Mater., vol. 25, no. 40, pp. 5714–5718, 2013.
[11] V. Zólyomi, N. D. Drummond, and V. I. Fal'Ko, Electrons and phonons in single layers of hexagonal indium chalcogenides from ab initio calculations, Phys. Rev. B - Condens. Matter Mater. Phys., vol. 89, no. 20, pp. 1–8, 2014.
[12] W. Feng, W. Zheng, W. Cao, and P. Hu, Back Gated Multilayer InSe Transistors with Enhanced Carrier Mobilities via the Suppression of Carrier Scattering from a Dielectric Interface, Adv. Mater., pp. 6587–6593, 2014.
[13] J. M. Gonzalez and I. I. Oleynik, Layer-dependent properties of SnS2 and SnSe2 two-dimensional materials, Phys. Rev. B, vol. 94, no. 12, pp. 1–10, (2016).
[14] A. Molina-Sánchez and L. Wirtz, "Phonons in single-layer and few-layer MoS2 and WS2," Phys. Rev. B - Condens. Matter Mater. Phys., vol. 84, no. 15, (2011).
[15] X. Chen, Z. Z. Lin, and M. Ju, "Controllable Band Alignment Transition in InSe–MoS 2 Van der Waals Heterostructure," Physica Status Solidi - Rapid Research Letters, vol. 12, no. 7. pp. 2–7, (2018).
[16] X. Li et al., "Type-II InSe/MoSe2(WSe2) van der Waals heterostructures: Vertical strain and electric field effects," J. Mater. Chem. C, vol. 6, no. 37, pp. 10010–10019, (2018).
[17] L. Yang et al., "Two-dimensional InSe/WS2 heterostructure with enhanced optoelectronic performance in the visible region," https://arxiv.org/abs/1808.01610, (2018).
[18] C. X. Xia et al., "Two-dimensional n-InSe/ p-GeSe(SnS) van der Waals heterojunctions: High carrier mobility and broadband performance," Phys. Rev. B, vol. 97, no. 11, pp. 1–9, 2018.
[19] J. E. Padilha, R. H. Miwa, A. J. R. Da Silva, and A. Fazzio, "Two-dimensional van der Waals p-n junction of InSe/phosphorene," Phys. Rev. B, vol. 95, no. 19, pp. 2–7, 2017.
[20] J.P. Perdew J P, K. Burke and M. Ernzerhof, Generalized gradient approximation made simple Phys. Rev. Lett. 77 (1996) 3865–3868.
[21] P. Giannozzi et. al. QUANTUM ESPRESSO: a modular and open-source software project for quantum simulations of materials., J. Phys. Condens. Matter. 21 (2009) 395502.
[22] H.J. Monkhorst and J.D. Pack, Special points for Brillouin-zone integrations Phys. Rev. B 13 (1976) 5188–5192.
[23] E.R. Davidson, Methods in Computational Molecular Physics edited by G.H.F. Diercksen and S. Wilson Vol. 113 NATO Advanced Study Institute, Series C (Plenum, New York, 1983), p. 95.
[24] N. Troullier, J.L. Martins, Efficient pseudopotentials for plane-wave calculations. II. Operators for fast iterative diagonalization, Phys. Rev. B. 43 (1991) 8861–8869.
[25] M. Fuchs, M. Scheffler, Ab initio pseudopotentials for electronic structure calculations of poly-atomic systems using density-functional theory, Comput. Phys. Commun. 119, (1999) 67-98 .
[26] S. Grimme, Semiempirical GGA-type density functional constructed with a long-range dispersion correction J. Comp. Chem. 27 (2006) 1787.
[27] J.D. Head, M.C. Zerner, A Broyden-Fletcher-Goldfarb-Shanno optimization procedure for molecular geometries, Chem. Phys. Lett. 122 (1985) 264–270.
[28] A. Benassi, A. Ferretti, C. Cavazzoni, PWSCF. 's epsilon.x user's manual.

[29] T.N. Todorov, Tight-binding simulation of current-carrying nanostructures, J. Phys. Condens. Matter 14 (2002) 3049–3084.
[30] J. Taylor, H. Guo, J. Wang, Ab initio modeling of quantum transport properties of molecular electronic devices, Phys. Rev. B 63 (2001) 245407.
[31] J. Taylor, H. Guo, J. Wang, Ab initio modeling of open systems: charge transfer, electron conduction, and molecular switching of a C60 device, Phys. Rev. B 63 (2001) 121104.
[32] Á. Szabó, Doctoral thesis: Dissipative quantum transport simulations in two-dimensional semiconductor devices from first principles (2016). https://doi.org/10.3929/ethz-a-010659234
[33] Synopsys QuantumATK, v 2016.4
[Online: https://www.synopsys.com/silicon/quantumatk.html]
[34] K.S. Thygesen and K.W. Jacobsen. Molecular transport calculations with wannier functions. Chemical Physics, 319, (2005)111 – 125.
[35] K. Stokbro, J. Taylor, M. Brandbyge, J.-L. Mozos, and P. Ordejón. Theoretical study of the nonlinear conductance of di-thiol benzene coupled to Au(1 1 1) surfaces via thiol and thiolate bonds. Computational Materials Science, 27, (2003),151 – 160.
[36] Supplementary Material for 'Electronic and optical properties of SnX2 (X=S, Se) - InSe van der Waal's heterostructures from first-principle calculations'.
[37] J. A. Hatchel, 'The Nanoscale Optical Properties of Complex Nanostructures', Springer Nature, Heidelberg, 2018. ISBN 978-3-319-70258-2